Aggregation-Induced Enhanced Emission of a Dimethylacridan Substituted Pyrimidine Derivative

Julien Massue, Lacina Diarra, Ioannis Georgoulis, Arnaud Fihey, Françoise Robin-Le Guen, Gilles Ulrich, Mihalis Fakis, Sylvain Achelle

ChemPhotoChem

Research Articles
doi.org/10.1002/cptc.202300085

Chemistry Europe
European Chemical Societies Publishing

www.chemphotochem.org

Aggregation-Induced Enhanced Emission of a Dimethylacridan Substituted Pyrimidine Derivative

Julien Massue,*[a] Lacina Diarra,[b] Ioannis Georgoulis,[c] Arnaud Fihey,[b] Françoise Robin-le Guen,[b] Gilles Ulrich,[a] Mihalis Fakis,*[c] and Sylvain Achelle*[b]

A pyrimidine chromophore bearing an acridan fragment was synthesized and its photophysical properties were studied. In solution, this compound is characterized by an important positive emission solvatochromism with a shift of 5800 cm^{-1} between nonpolar heptane and dichloromethane (DCM) associated with large Stokes shifts (up to 9100 cm^{-1} in DCM). Mono-exponential fluorescence decays are observed in heptane whereas more complicated bi- or three-exponential decays are observed in more polar solvents due to an interplay between locally excited and charge transfer excited state. Additionally, an aggregation-induced enhanced emission process was demonstrated in THF/water mixtures. At low temperature (77 K), in a polymethylmethacrylate (PMMA) thin film, the presence of an accessible triplet state (T1) was demonstrated, which was not observed in solution. Finally, we show that it is possible to protonate the chromophore in thin film leading to panchromatic dual emission

Introduction

Pyrimidine push-pull derivatives have been intensively studied for their charge-transfer based environment-responsive photoluminescence properties.[1] Indeed, the pyrimidine ring is a heterocyclic core with a strong electron-withdrawing character due to its π-deficient nature, and two electronic lone pairs, prone to interact with electrophiles. Interestingly, it is known that the photophysics of pyrimidine and pyrimidine-based chromophores is highly sensitive to the physical properties of their environment.[2] In particular, it has been demonstrated that in acidic media, a significant modification of the emission properties can be observed, due to the protonation of one of the nitrogen atoms of the pyrimidine fragment.[3] An emission quenching or a bathochromic shift of the emission band can be observed, due to the reinforcement of the electron-withdrawing character of the pyrimidine core upon protonation that enhances the intramolecular charge transfer (ICT).[3] In some selected cases, when protonation is only partial, a panchromatic dual emission of white light can be observed.[4] Pyrimidines that are substituted by carbazole or amino electron-donating groups via phenylene linkers are generally characterized by high photoluminescence quantum yield (PLQY) in solution.[5]

Organic light-emitting diodes (OLEDs) are currently the subject of extensive research for their use in displays and lighting.[6] In this context, pyrimidine derivatives have been widely used as emitters, either involved in Iridium(III)[7] or Platinum(II)[8] complexes for phosphorescent OLEDs or as thermally activated delayed fluorescence (TADF) derivatives for third generation OLEDs.[9] Reported pyrimidine-based TADF chromophores generally embed one or more sterically hindered nitrogen-containing groups, such as acridan, phenoxazine or phenothiazine, attached through phenylene linkers.[9,10] In case of less electron donating carbazolyl group in *para* position, phenylpyrimidine generally does not exhibit TADF properties.[11] Steric hindrance is indeed required to provide an orthogonal configuration of the electron-donating group with respect to the pyrimidine scaffold, reducing the overlap between the highest occupied molecular orbital (HOMO) and the lowest unoccupied molecular orbital (LUMO), thereby favoring a small singlet-triplet energy splitting (ΔE_{ST}), indispensable for the observation of TADF.[12] Ganesan and coworkers have designed 6-(4-[9,9-Dimethyl-9,10-dihydroacridinyl]phenyl)-2,4-diphenylpyrimidine and spiro-[acridine-9,90 -fluorene] analogue chromophores that exhibited mechanochromism, TADF properties and were used as emitter

[a] *Dr. J. Massue, Dr. G. Ulrich*
Institut de Chimie et Procédés pour l'Energie, l'Environnement et la Santé (ICPEES), Equipe Chimie Organique pour la Biologie, les Matériaux et l'Optique (COMBO), UMR CNRS 7515, 25 Rue Becquerel, 67087 Strasbourg, France
E-mail: massue@unistra.fr
Homepage: http://icpees.unistra.fr/chimie-moleculaire-et-analytique/mari/personnel/julien-massue/

[b] *L. Diarra, Dr. A. Fihey, Prof. F. Robin-le Guen, Dr. S. Achelle*
Univ Rennes, CNRS ISCR (Institut des Sciences Chimiques de Rennes) UMR 6226, 35000, Rennes, France
E-mail: sylvain.achelle@univ-rennes.fr
Homepage: https://iscr.univ-rennes.fr/sylvain-achelle

[c] *I. Georgoulis, Prof. M. Fakis*
Department of Physics, University of Patras, 26500 Patras, Greece
E-mail: fakis@upatras.gr
Homepage: http://www.physics.upatras.gr/en/faculty/fakis/

Supporting information for this article is available on the WWW under https://doi.org/10.1002/cptc.202300085

for blue OLED with EQE up to 14.2%.[13] Whereas many fluorophores are highly emissive in dilute solution, they often exhibit fluorescence aggregation-caused quenching (ACQ) in the solid-state, which limits their practical application as solid-state emitters. On the other hand, some rotor-shaped chromophores display strong fluorescence quenching in solution but a restriction of intramolecular rotations[14] in the solid-state leads to significant enhancement of emission intensity.[15] This phenomenon, called Aggregation Induced Emission (AIE) or Aggregation Induced Enhanced Emission (AIEE), depending on the complete or partial quenching of luminescence in solution, has been observed on a large structural range of molecular structures.[16] In this context, we have recently described a selection of acridan-substituted styrylpyrimidine derivatives with AIE characteristics and dual emission in polar solvents.[17]

In this contribution, we present an original pyrimidine-based derivative substituted by a sterically hindered acridan fragment but also by additional biaryl moieties, in order to further enhance its AIEE behavior (Figure 1). The photophysical properties, as well as AIEE studies of pyrimidine **1** have been fully investigated experimentally, in solution and in the solid-state as thin films. Moreover, TD-DFT calculations have also been performed to ascertain the nature of the transitions involved.

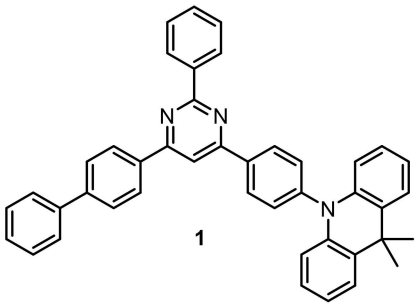

Figure 1. Pyrimidine **1** studied in this article.

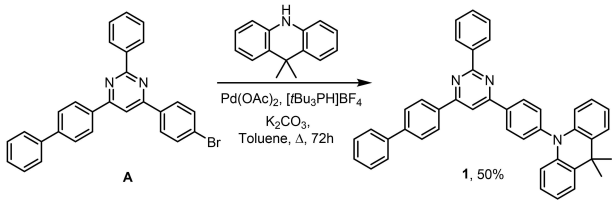

Scheme 1. Synthesis of pyrimidine **1**.

Results and Discussion

Synthesis

Target compound **1** was obtained by Pd-catalyzed Buchwald cross-coupling reaction from commercially available reagents 4-(biphenyl-4-yl)-6-(4-bromophenyl)-2-phenylpyrimidine **A** and 9,9-dimethylacridan in 50% yield after purification by silica gel column chromatography followed by recrystallization (Scheme 1). Pyrimidine derivative **1** was fully characterized by ^{1}H, ^{13}C NMR spectroscopy, as well as HR-MS (see the experimental part).

Photophysical properties in solutions

The photophysical properties for pyrimidine derivative **1** were recorded in solution in multiple solvents of different polarities and in the solid-state, as 1% wt doped in poly(methyl methacrylate) (PMMA) thin films. The photophysical data are summarized in Table 1.

In solution, pyrimidine dye **1** displays very similar absorption profiles in all solvents, i.e., intense bands below 300 nm corresponding to π-π^* transitions of the aromatic rings with a shoulder at ~310 nm (Figure 2). An additional absorption band with low intensity is observed at lower energies around 370 nm and can be tentatively attributed to a transition towards a CT state, owing to the presence of a strong push-pull structure. The molar absorption coefficients of these bands are in the $2 \cdot 10^3\ M^{-1}\ cm^{-1}$ range (Table 1). Photoexcitation in this CT absorption band leads to the observation of fluorescence in all solvents at room temperature (see Figure 2 for the fluorescence spectra in heptane and toluene). An important positive emission solvatochromism is observed upon increasing the solvent polarity (Figure 3). Specifically, the emission maximum is bathochromically shifted from 422 nm in heptane to 562 nm in dichloromethane (DCM). Emission intensity is dramatically decreased in more polar solvents such as acetonitrile (MeCN).

Table 1. Photophysical data for pyrimidine **1** in solution and in thin films.

Solvent/matrix	λ_{abs}[a] [nm] (ε[b] [$mM^{-1}\ cm^{-1}$])	λ_{em}[c] [nm]	Δss[e] [cm^{-1}]	Φ_f[f]	τ[g] [ns]
heptane	278 (51.9), 312 (21.5), 372 (1.7)	422 (422)[d]	3300	0.11	4.07
Toluene	276 (50.5), 313 (21.8), 372 (1.9)	474 (422)[d]	5800	0.15	1.56 (0.20), 9.56 (0.80)
1,4-dioxane	278 (47.5), 313 (23.2,) 373 (2.1)	500	6800	0.26	0.25 (0.61), 1.00 (0.37), 5.13 (0.02)
THF	276 (47.5), 313 (19.2), 372 (2.0)	535	8200	0.10	1.82 (0.13), 12.32 (0.87)
DCM	278 (51.8), 313 (30.2), 372 (2.2)	562	9100	0.24	17.95
PMMA[h]	–	450(432/483)[d]	–	–	1.40 (0.34), 6.30 (0.37), 14.41 (0.29)

[a] Wavelength of absorption maximum at 298 K, [b] Molar absorption coefficient at 298 K, [c] Wavelength of emission maximum at 298 K, [d] Wavelength of emission maximum at 77 K in deaerated solutions, [e] Stokes shift, [f] Relative quantum yield determined in solution at 298 K using 9,10-bisphenylethynylanthracene in cyclohexane ($\Phi_f = 1.00$) as a reference,[19] [g] lifetimes recorded at 298 K, the pre-exponential factors are shown in parentheses, [h] doped in Poly(methylmethacrylate) (PMMA) 1% wt.

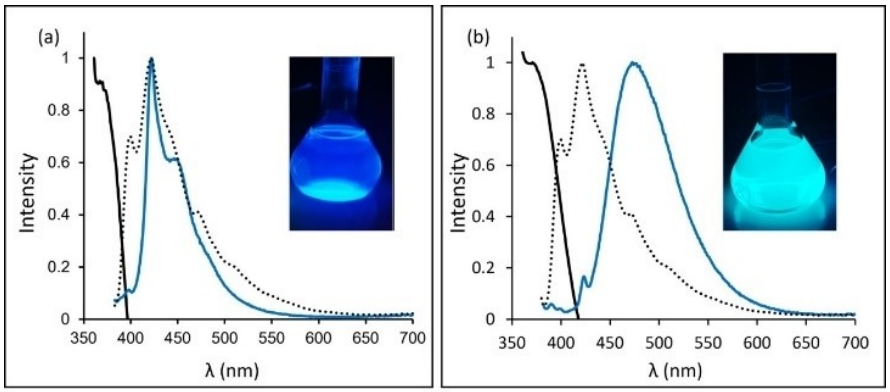

Figure 2. Normalized absorption (plain black), emission at 298 K (plain blue) and emission at 77 K (dotted black) of pyrimidine **1** in (a) heptane and (b) toluene. Inset: photographs of solutions of **1** in heptane and in toluene at 298 K under irradiation (λexc = 365 nm), $c = 10$ μM.

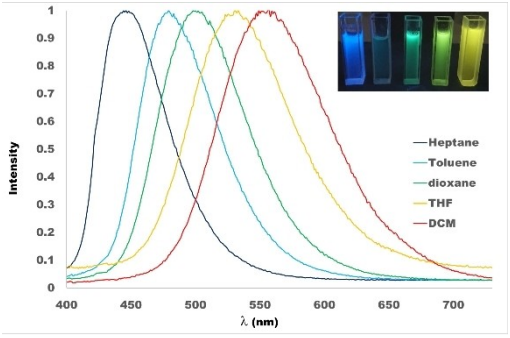

Figure 3. Normalized emission spectra of pyrimidine **1** in a series of solvents with different polarity at 298 K Inset: photographs of solutions of **1** in heptane, toluene, 1,4-dioxane, THF and DCM (from left to right) at 298 K under irradiation ($\lambda_{exc} = 365$ nm), $c = 10$ μM.

This positive emission solvatochromism, which is characteristic of push-pull derivatives, is explained by the stabilization of the highly polar emitting excited state in polar solvents.[18] This marked solvatochromic range, spanning 5800 cm^{-1} between heptane and DCM, combined with large Stokes Shifts ($>$9000 cm^{-1} in DCM) could indicate the presence of a twisted intramolecular charge transfer (TICT) excited state. The quantum yields are in the range 0.10–0.26, highlighting the presence of strong non-radiative deactivations, consistent with the presence of free rotations around the peripheral aryl rings. As expected the emission properties in various media are close to those reported for 6-(4-[9,9-Dimethyl-9,10-dihydroacridinyl]phenyl)-2,4-diphenylpyrimidine analogue.[13a]

To shed more light on the nature of the emissive transition, emission spectra in heptane and toluene were also recorded at 77 K (Figure 2). Freezing the solution in heptane led to a structured emission spectrum with the same maximum wavelength as at 298 K ($\lambda_{em} = 422$ nm), whereas, in toluene, at 77 K, a strong blue shift is observed for the emission band ($\lambda_{em} = 422$ nm at 77 K vs. 474 nm at 298 K). These observations lead us to conclude that in heptane, the lowest excited state would be of pure singlet nature (^{1}LE), while in the more polar toluene, emission would also involve some contribution from a CT-controlled excited state (^{1}CT).

The fluorescence decays of compound **1** in all solvents have been measured in the ns timescale and the results are shown in Figure 4 while the fitting parameters are summarized in Table 1. In heptane, **1** exhibits a single exponential decay with time constant of 4.07 ns attributed to the lifetime of the ^{1}LE state. By increasing the solvent polarity, the dynamics become more complicated and are fitted by a bi- or three-exponential function. In toluene and THF, two decay mechanisms are found of 1.5–1.8 ns (with pre-exponential factors of 0.13–0.20) and of 9.5–12.3 ns time-constants (with pre-exponential factors of 0.80–0.87). The fast mechanism could be due to a quenched ^{1}LE state emission while the long one can be attributed to a relaxed excited state of CT character. In DCM, in which the largest Stokes shift is observed, the emission from the ^{1}LE state is totally absent in the decays and the emission of the relaxed CT state is only present with a lifetime of ~18 ns. Finally, in 1,4-dioxane, being a solvent of intermediate polarity among those used here, the dynamics are complicated and three lifetimes are found. These are shorter than in the other solvents pointing to a quenching of the excited state and increased non-radiative transitions.

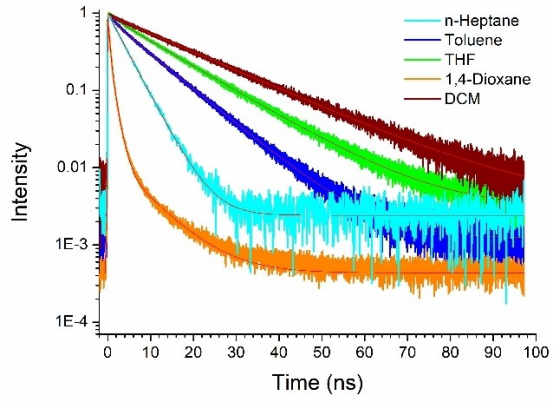

Figure 4. Fluorescence decays of **1** in various solvents. The detection was made at the peaks of the fluorescence spectra ($\lambda_{exc} = 400$ nm).

Photophysical properties in solid state films

Emission spectra in the solid-state were also recorded at 298 K and 77 K for pyrimidine **1**, as 1% wt doped in PMMA thin films (Figure 5a). After excitation at 298 K, a broad single emission band is observed with a peak at 450 nm which is between the emission peaks found in heptane and toluene. Freezing the film down to 77 K led to a hypsochromic shift of this band (λ_{em} = 432 nm), along with the appearance of a second red-shifted shoulder at 483 nm. This additional band, which was not observed in solution at room or low temperature, could be attributed to the presence of an accessible triplet state (T_1) in the solid state. To confirm this hypothesis, a phosphorescence spectrum was recorded for PMMA thin films at room temperature (time delay = 0.1 ms), leading to the observation of a single band at 475 nm, with an estimated lifetime of 0.43 ms. The good overlap between these two emission bands (λ_{em} = 475/483 nm) provides evidence on the population of a low-lying phosphorescent T_1 state for **1**, but only in films, not in solution, neither at 298 nor at 77 K. The above clearly points out the importance of the environment on the stabilization of the triplet state. Additionally, protonation studies were performed on PMMA thin films of **1** by dipping the film in HCl vapors for 10 minutes. A progressive color change of the films from transparent to red was gradually observed and seemed to be complete after 5 minutes. At 298 K, a dual emission was observed (λ_{em} = 432/574 nm) (Figure 5b), consistent with the monoprotonation of the pyrimidine ring, enhancing the CT character and red-shifting the emission band.[3] At 77 K, the same dual emission is recorded (λ_{em} = 435/574 nm) but with a different intensity ratio between the two bands.

AIEE Studies

The AIEE properties of compound **1** were studied in mixtures of THF (good solvent) and water (poor solvent). Figure 6 shows the emission spectra in various THF/water ratios. When the water ratio is gradually increased up to 60% a progressive decrease of the emission intensity associated with a bathochromic shift of the emission band is observed: this is due to the increase of the polarity of the media. Then, a progressive increase of the emission intensity associated with a hypsochromic shift is observed due to the formation of aggregates. The maximum emission intensity is achieved for a water ratio of 80%. In solution with more than 80% water, a hypsochromic

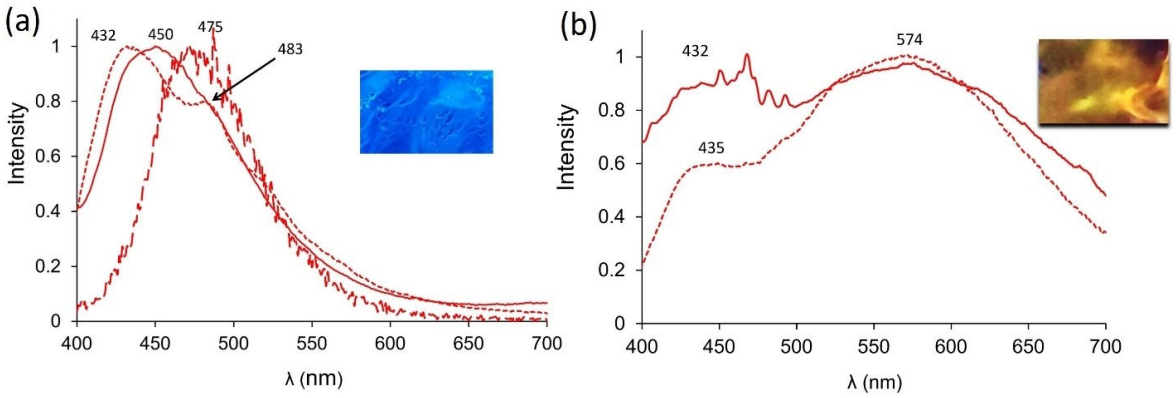

Figure 5. (a) Steady-state emission spectra of **1** in PMMA thin films at 298 K (plain) and 77 K (dotted) and phosphorescence emission of **1** at 298 K (dashed) and (b) Steady-state emission spectra of **1.H+** in PMMA thin films at 298 K (plain) and 77 K (dotted) (λ_{exc} = 370 nm). The insets show photographs of the films before and after protonation under irradiation (λ_{exc} = 365 nm).

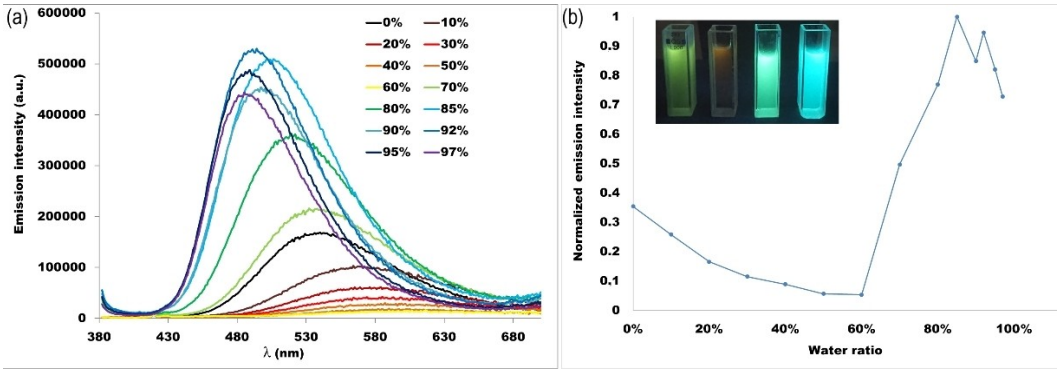

Figure 6. (a) Fluorescence emission spectra in a mixture of THF/water (b) integrated emission band in normalized units versus volume percentage of water in mixtures of THF/water. Inset: photographs of solutions of **1** in mixtures of THF/water with different ratio of water: 0%, 50% 75% 97% (from left to right) at 298 K under irradiation (λexc = 365 nm).

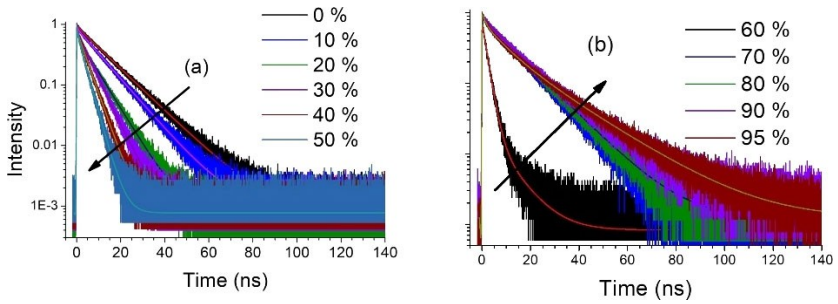

Figure 7. Fluorescence decays of compound **1** in mixtures of THF/water with increasing ratio of water (a) 0–50% and (b) 60–95%.

shift is still observed but the emission intensity slightly decreases.

Figure 7 shows the fluorescence decays of pyrimidine **1** in mixtures of THF/water. Specifically, Figures 7a and 7b show the decays for water percentage of 0 to 50% and 60% up to 95% respectively. All decays have been fitted with multi-exponential functions and the fitting parameters are given in Table S1. The first observation is that upon increasing the water percentage from 0 to 50%, the decays monotonically become faster while both time-constants used to fit the decays decrease (Table S1). For a water percentage of 60%, the average lifetime almost remains unchanged, while the lifetimes start to increase for larger amounts of water. In total, the average lifetime decreases from 11.22 ns in pure THF solution to 2.11 ns in THF/water 60%. Further increasing the water percentage to 70%, leads to a dramatic increase of the average lifetime from 2.11 ns to 10.0 ns, suggesting an enhancement of the radiative transitions, as compared to the non-radiative ones. A further increase of the water percentage does not lead to significant changes of the average lifetime. It should be noted that the steady-state emission intensity also increases at exactly the same percentage (70%) which can be considered as the critical water amount for aggregation formation. The increase of the excited-state lifetime in compound **1** upon aggregation, is related to the suppression of the energy-consuming out-of-plane rotations which is in favor of radiative transitions.

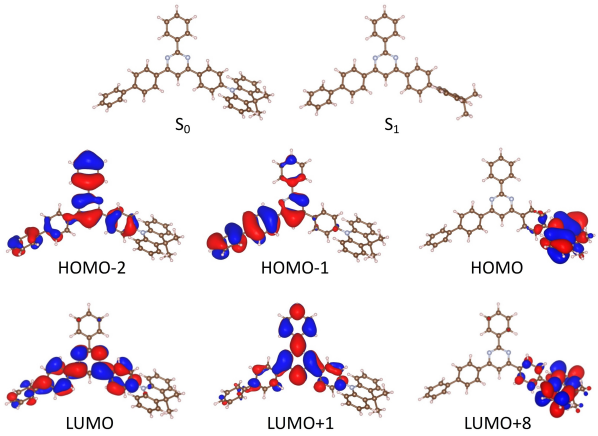

Figure 8. Ground-state and first excited-state geometries and frontier orbitals (isovalue of 0.02 a.u.) involved in the electronic relevant transitions.

Table 2. Computed optical properties of pyrimidine 1 in DCM. See computational section for more details.

λ_{abs} (nm)	*f*	$S_0 \rightarrow S_n$	Orbital decomp.	λ_{em} (nm), $S_1 \rightarrow S_0$	*f*
469	0.00	$S_0 \rightarrow S_1$	HOMO→LUMO	562	0.00
338	0.80	$S_0 \rightarrow S_3$	HOMO-1→LUMO	–	–
311	0.25	$S_0 \rightarrow S_7$	HOMO-1→LUMO+1	–	–
305	0.12	$S_0 \rightarrow S_9$	HOMO-1→LUMO+1 HOMO-2→LUMO	–	–
299	0.27	$S_0 \rightarrow S_{11}$	HOMO→LUMO+8	–	–

DFT studies

All following results are presented using a DFT protocol resulting in a satisfying agreement with both the experimental absorption and emission spectra (see Computational details section for more information, and Table S2 for a comparison of DFT methods). The computed ground-state structure of **1** (see Figure 8) in DCM exhibits a high torsion angle (89°) between the dimethylacridan and the phenyl unit bridging to the pyrimidine cycle. From this ground-state, the first electronic transition computed at 469 nm in DCM (see Table 2) possesses a complete π-π* charge transfer character and thus a zero oscillator strength, in line with the low-lying absorption band measured at 372 nm. Frontier orbitals involved, depicted in Figure 8, are decorrelated and located respectively on the dimethylacridan donor moiety for the HOMO and on the pyrimidine acceptor part for the LUMO (along with a phenyl contribution) as observed for analogue compounds.[13a] Transitions of higher energy possess a non-negligible oscillator strength and correspond to localized π-π* excitations. The most intense one is found at 338 nm (and compares with the second absorption band at 313 nm) and involves occupied and virtual orbitals delocalized on the pyrimidine and phenyl units (HOMO-1 and LUMO). In the 310–300 nm range, three relatively intense transitions are obtained, that correlate with the experimental band at 278 nm. The computed transitions at 311 nm and 305 nm possess a similar pyrimidine/phenyl character, while the transition at 299 nm involves the dimethylacridan (see Table 2 and Figure 8).

After relaxation in the first excited state, **1** undergoes a planarization of its core. The torsion angle between the phenyl rings and the pyrimidine cycle decreases from ca. 25° in the

ground state to ca. 0° in the excited state in DCM. Nevertheless, the torsion angle between the dimethylacridan and the phenyl linked to the pyrimidine ring remains at 90°. Emission of **1** from this excited state is computed at 562 nm in DCM, well in line with the experimental value. Due to the conservation of the perpendicular donor/acceptor conformation, this transition exhibits a null oscillator strength, as for the absorption. This static CT picture of the first (de−)excitation may be counterbalanced by the possible donor (dimethylacridan)/acceptor (phenyl-pyrimidine) rotation at room temperature and could explain the non-negligible quantum yield of fluorescence. Scanning the S_1 state along this dihedral angle reveals a relatively small 7.6 kcal/mol energy difference between the fully perpendicular (90°) and the twisted (45°) S_1 geometry. The AIEE features observed are also expected to arise from this effect once the aggregation constrains the torsion. An optimized S_1 with a 45° constraint leads to an electronic transition to S_0 with an increased oscillator strength of 0.25 and blue shifted to 541 nm, in line with the experimental changes in the spectra upon water addition. Frontier molecular orbitals in this constrained conformation are depicted in Figure S1, showing a recovery of a degree of p-delocalization between the dimethylacridan and the phenyl/diazine core.

Conclusions

In conclusion, we have synthesized and fully analyzed the photophysical and computational properties of a novel pyrimidine-based derivative functionalized with a dimethylacridan moiety. This compound displays a pronounced emission solvatochromic optical behavior with emission bands spanning a large range, between heptane and DCM. This charge-transfer controlled fluorescence was further evidenced at 77 K where a marked blue-shift is observed in toluene, owing to the unfavorable alignment of dipoles at low temperature. The emission in thin films (pyrimidine doped in PMMA) was also analyzed and revealed the presence of a low-lying triplet state which was not observed in solution. Additionally, the studied chromophore displays interesting AIEE features, as evidenced by an increase of fluorescence intensity in THF/water mixtures. While displaying lifetime in the nanosecond range, this study will help to establish ground rules for the future development of pyrimidine-based dyes with TADF behavior. Work along these lines is currently in progress.

Experimental part

Materials and methods

All solvents were reagent grade for synthesis. Starting materials were purchased from Sigma-Aldrich or TCI and were used without further purification. Thin layer chromatography (TLC) was conducted on pre-coated aluminum sheets with 0.20 mm Merck Alugram SIL G/UV254 with fluorescent indicator UV254 and 0.25 mm Merck silica gel (60-F254). Column chromatography was carried out using Acros silica gel 60 (particle size 63–200 μm).

NMR spectra were recorded in $CDCl_3$ on a Bruker AC-300 spectrometer. The chemical shifts δ are reported in ppm and are referenced to the appropriate solvent signals of $CDCl_3$ (1H, $\delta =$ 7.27 ppm; 13 C, $\delta = 77.0$ ppm). The coupling constants J are given in Hz. In the 1H NMR spectra, the following abbreviations are used to describe the peak patterns: s (singlet), d (doublet), t (triplet), q (quadruplet), m (multiplet). Acidic impurities in $CDCl_3$ were removed by treatment with solid K_2CO_3. High-resolution mass analyses were carried out at the 'Centre Régional de Mesures Physiques de l'Ouest' (CRMPO, Université de Rennes 1) using a Bruker MicroTOF-Q II instrument.

Absorption spectra were recorded using a dual-beam grating Schimadzu UV-3000 absorption spectrometer with a quartz cell of 1 cm of optical path length. The steady-state fluorescence emission spectra were recorded by using a Horiba S2 Jobin Yvon Fluoromax 4 or a Spex Fluoromax-3 Jobin-Yvon Horiba spectrofluorimeter. All fluorescence and excitation spectra were corrected to take into account the response of the photomultiplier. Fluorescence quantum yields (±10%) were determined relative to the indicated reference. PMMA films were prepared by mixing 1% wt (1 mg) of pyrimidine 1 with PMMA (100 mg) in THF and by subsequent drop casting method. For time resolved fluorescence measurements in the ps-ns timescale, the Time Correlated Single Photon Counting (TCSPC) technique has been used based on a FluoTime 200 spectrometer (Picoquant).[20] The excitation source was a ps diode laser emitting 60 ps pulses at 400 nm and the IRF was ~80 ps. The samples for steady state and fluorescence dynamics measurements were dilute solutions with an optical density (O.D.) of ~0.1 at excitation wavelength.

Computational details

All DFT calculations were conducted with the Gaussian 16 suite.[21] Geometry optimizations of the ground states were systematically followed by frequencies calculations to ensure the validity of the minima. UV-Visible absorption spectra were simulated through TD-DFT, by computing the first 15 electronic excitations. Emission properties were obtained by optimizing the first excited state, followed by frequencies calculations, as for the ground state. To simulate the impact of the donor-acceptor twist on emission, excited state optimizations were constrained with a fix phenyl/dimethylacridan dihedral angle of 60° and 45°, while allowing the other geometric parameters to relax. To pinpoint solvent effects, all these steps have been conducted with a PCM model[22] of DCM. Results presented in the main text have been obtained with the B3LYP functional and a 6-311 + G(d,p) basis set, to reproduce the experimental trends. Additionally, a comparison between this computational Scheme, a meta-hybrid GGA with a higher HF exchange (M062X) and a range-separated hybrid functional with dispersion (wB97xD) is presented in ESI (Table S2).

Synthesis

4-([1,1′-biphenyl]-4-yl)-6-(4-[9,9-Dimethyl-9,10-dihydroacridinyl]phenyl)-2-phenylpyrimidine (**1**): A stirred mixture of 4-(biphenyl-4-yl)6-(4-bromophenyl)2-phenylpyrimidine (463 mg, 1 mmol), 9,9-dimethyl-9,10-dihydroacridine (230 mg, 1.1 mmol) and potassium carbonate (414 mg, 3 mmol) in degassed toluene (5 mL) was left under nitrogen atmosphere with stirring for 30 min before adding palladium(II) acetate(25 mg, 0.1 mmol) and tri-*tert*-butylphosphine tetrafluoroborate (35 mg, 0.12 mmol). the reaction mixture was then heated to reflux under nitrogen for 72 h in a Schlenk tube. The reaction mixture was cooled, filtered, and dissolved with a 1:1 mixture of CH_2Cl2 and water (50 mL) and the organic layer was separated. The aqueous layer was extracted with

CH_2Cl_2 (2×25 mL). The organic phases were combined, dried and evaporated. The residue was purified by silica gel column chromatography (CH_2Cl_2/petroleum ether 1:1) and recrystallisation from DCM/heptane. Pale yellow solid. Yield: 50% (143 mg) ^{1}H NMR (300 MHz, $CDCl_3$) δ: 8.81 (dd, 2H, ^3J=8.1 Hz, ^4J=2.1 Hz), 8.59 (d, 2H, ^3J=8.4 Hz), 8.46 (d, 2H, ^3J=8.4 Hz), 8.18 (s, 1H), 7.85 (d, 2H, ^3J=8.4 Hz), 7.73 (d, 2H, ^3J=8.4 Hz), 7.63–7.44 (m, 10H), 7.06–6.96 (m, 4H), 6.40 (dd, 2H, ^3J=7.5 Hz, ^4J=1.2 Hz), 1.76 (s, 6H), ^{13}C NMR (75 MHz, $CDCl_3$) δ 164.8, 164.6, 164.0, 143.8, 140.7, 140.3, 138.0, 137.5, 136.2, 131.9, 130.8, 130.2, 129.9, 128.9, 128.5, 127.9, 127.8, 127.7, 127.2, 126.4, 120.8, 114.1, 110.3. 36.0, 31.3 HRMS (ESI/ASAP, TOF) m/z calculated for $C_{43}H_{34}N_3$ (M^+)•592.2747 found 592.2747.

Acknowledgements

The authors acknowledge the CNRS for financial support. A. F. is grateful for the calculation resources support through the French GENCI agency at the CINES and IDRIS centers (grants: A0100800649 and AD010800649R1).

Conflict of Interests

The authors declare no conflict of interest.

Data Availability Statement

The data that support the findings of this study are available in the supplementary material of this article.

Keywords: aggregation-induced enhanced emission · intramolecular charge transfer · photophysics · pyrimidine molecules · time-resolved spectroscopy

[1] a) S. Achelle, J. Rodríguez-López, F. Robin-le Guen, *Org. Biomol. Chem.* **2023**, *21*, 39–52; b) S. Achelle, J. Rodríguez-López, F. Robin-le Guen, *ChemistrySelect* **2018**, *3*, 1852–1886.
[2] a) R. Wang, H. Fan, Y. Mu, M. Li, S. Pu, *Dyes Pigm.* **2022**, *208*, 110808; b) E. V. Verbitskiy, G. L. Rusinov, O. N. Chupakhin, V. N. Charushin, *Dyes Pigm.* **2020**, *180*, 108414; c) J. Rodríguez-Aguilar, M. Vidal, C. Pastenes, C. Aliaga, M. C. Rezende, M. Domínguez, *Photochem. Photobiol.* **2018**, *94*, 1100–1108; d) S. Achelle, J. Rodríguez-López, F. Bureš, F. Robin-le Guen, *Dyes Pigm.* **2015**, *121*, 305–311.
[3] S. Achelle, J. Rodríguez-López, F. Bureš, F. Robin-le Guen, *Chem. Rec.* **2020**, *20*, 440–451.
[4] a) S. Achelle, J. Rodríguez-López, M. Larbani, R. Plazza-Pedroche, F. Robin-le Guen, *Molecules* **2019**, *24*, 1742; b) S. Achelle, J. Rodríguez-López, N. Cabon, F. Robin-le Guen, *RSC Adv.* **2015**, *5*, 107396–107399.
[5] a) D. G. Slobodinyuk, A. I. Slobodinuyk, V. N. Strelnikov, E. V. Shklyaeva, G. G. Abashev, *ChemistrySelect* **2022**, *7*, e202203180; b) C. Pérez-Caaveiro, M. Moreno Oliva, J. T. López Navarrete, J. Pérez Sestelo, M. Montserrat Martínez, L. A. Sarandeses, *J. Org. Chem.* **2019**, *85*, 8870–8885; c) S.-i. Kato, Y. Yamada, H. Hiyoshi, K. Umezu, Y. Nakamura, *J. Org. Chem.* **2015**, *80*, 9076–9090; d) L. Skardziute, J. Dodonova, A. Voitechovicius, J. Jovaisaite, R. Komskis, A. Voitechoviciute, J. Bucevicius, K. Kazlauskas, S. Jursenas, S. Tumkevicius, *Dyes Pigm.* **2015**, *118*, 118–128.
[6] a) Y. Liu, C. Li, Z. Ren, S. Yan, M. R. Bryce, *Nat. Rev. Mater.* **2018**, *3*, 18020 ; b) P.-T. Chou, Y. Chi, *Chem. Eur. J.* **2007**, *13*, 380–395.
[7] a) Y.-K. Chen, H.-H. Kuo, D. Luo, Y.-N. Lai, W.-C. Li, C.-H. Chang, D. Escudero, A. K.-Y. Jen, L.-Y. Hsu, Y. Chi, *Chem. Mater.* **2019**, *31*, 6453–6464; b) L.-S. Cui, Y. Liu, X.-Y. Liu, Z.-Q. Jiang, L.-S. Liao, *ACS Appl. Mater. Interfaces* **2015**, *7*, 11007–11014.
[8] a) M. Z. Shafikov, P. Pander, A. V. Zaytsev, R. Daniels, R. Martinscroft, F. B. Dias, J. A. G. Williams, V. N. Kozhevnikov, *J. Mater. Chem. C* **2021**, *9*, 127–135; b) M. Z. Shafikov, R. Daniels, P. Pander, F. B. Dias, J. A. G. Williams, V. N. Kozheynikov, *ACS Appl. Mater. Interfaces* **2019**, *11*, 8182–8193; c) J. Zhao, F. Dang, Z. Feng, B. Liu, X. Yang, Y. Wu, G. Zhou, Z. Wu, W.-Y. Wong, *Chem. Commun.* **2017**, *53*, 7581–7584.
[9] a) S. Achelle, M. Hodée, J. Massue, A. Fihey, C. Katan, *Dyes Pigm.* **2022**, *200*, 110157; b) I. Fiodorova, T. Serevicius, R. Skaigiris, S. Jursenas, S. Tumkevicius, *Beilstein J. Org. Chem.* **2022**, *18*, 497–507; c) U. Tsiko, D. Volyniuk, V. Andruleviciene, K. Leitonas, G. Sych, O. Bezvikonnyi, V. Jasinskas, V. Gulbinas, P. Stakhira, J. V. Grazulevicius, *Mater. Today Chem.* **2022**, *25*, 100955; d) R. Komatsu, H. Sasabe, J. Kido, *J. Photonics Energy* **2018**, *8*, 032108.
[10] a) T. Serevičius, R. Skaigiris, J. Dodonova, L. Jagintavičius, D. Banevičius, K. Kazlauskas, S. Tumkevičius, S. Juršėnas, *ACS Appl. Mater. Interfaces* **2020**, *12*, 10727–10736; b) R. Komatsu, H. Sasabe, Y. Seino, K. Nakao, J. Kido, *J. Mater. Chem. C* **2016**, *4*, 2274–2278 ; c) K. Wu, T. Zhng, L. Zhan, C. Zhong, S. Gong, N. Jiang, Z.-H. Lu, C. Yang, *Chem. Eur. J.* **2016**, *22*, 10860–10866.
[11] T. Serevičius, J. Dodonova, R. Skaigiris, D. Banevičius, K. Kazlauskas, S. Juršėnas, S. Tumkevicius, *J. Mater. Chem. C* **2020**, *8*, 11192–11200.
[12] a) R. Dhali, D. K. A. Phan Huu, F. Bertocchi, C. Sissa, F. Terenziani, A. Painelli, *Phys. Chem. Chem. Phys.* **2021**, *23*, 378–387; b) M. Y. Wong, E. Zysman-Colman, *Adv. Mater.* **2017**, *29*, 1605444; c) Y. Tao, K. Yuan, T. Chen, P. Xu, H. Li, R. Chen, C. Zhrng, L. Zhang, W. Huang, *Adv. Mater.* **2014**, *26*, 7931–7958.
[13] a) P. Ganesan, R. Ranganathan, Y. Chi, X.-K. Liu, C.-S. Lee, S.-H. Liu, G.-H. Lee, T.-C. Lin, Y.-T. Chen, P.-T. Chou, *Chem. Eur. J.* **2017**, *23*, 2858–2866; b) P. Ganasan, D.-G. Chen, J.-L. Liao, W.-C. Li, Y.-N. Lai, D. Luo, C.-H. Chang, C.-L. Ko, W.-Y. Hung, S.-W. Liu, G.-H. Lee, P.-T. Chou, Y. Chi, *J. Mater. Chem. C* **2018**, *6*, 10088–10100.
[14] Q. Zeng, Z. Li, Y. Dong, C. Di, A. Qin, Y. Hong, L. Ji, Z. Zhu, C. K. W. Jim, G. Yu, Q. Li, Y. Liu, J. Qin, B. Z. Tang, *Chem. Commun.* **2007**, *1*, 70–72.
[15] a) J. Mei, N. L. C. Leung, R. T. K. Kwok, J. W. Y. Lam, B. Z. Tang, *Chem. Rev.* **2015**, *115*, 11718–11940 ; b) B.-K. An, J. Gierschner, S. Y. Park, *Acc. Chem. Res.* **2012**, *45*, 544–554.
[16] a) H.-T. Feng, Y.-X. Yuan, J.-B. Xiong, Y.-S. Zheng, B. Z. Tang, *Chem. Soc. Rev.* **2018**, *47*, 7452; b) P. Shen, Z. Zhuang, Z. Zhao, B. Z. Tang, *J. Mater. Chem. C* **2018**, *6*, 11835; c) T. Stoerkler, P. Retailleau, D. Jacquemin, G. Ulrich, J. Massue, *Chem. Eur. J.* **2023**, *29*, e202203766.
[17] M. Fecková, I. K. Kalis, T. Roisnel, P. le Poul, O. Pytela, M. Klikar, F. Robin-le Guen, F. Bureš, M. Fakis, S. Achelle, *Chem. Eur. J.* **2021**, *27*, 1145–1159.
[18] a) R. Lartia, C. Allain, G. Bordeau, F. Schmidt, C. Fiorini-Debuisschert, F. Charra, M.-P. Teulade-Fichou, *J. Org. Chem.* **2008**, *73*, 1732–1744 ; b) C. Katan, M. Charlot, O. Mongin, C. Le Droumaguet, V. Jouikov, F. Terenziani, E. Badaeva, S. Tritiak, M. Blanchard-Desce, *J. Phys. Chem. B* **2010**, *114*, 3152–3169.
[19] M. Tanigushi, J. S. Lindsey, *Photochem. Photobiol.* **2018**, *94*, 290–327.
[20] N. Droseros, K. Seintis, M. Fakis, S. Gardelis, A. Nassiopoulou, *J. Lumin.* **2015**, *167*, 333–338.
[21] M. J. Frisch, G. W. Trucks, H. B. Schlegel, G. E. Scuseria, M. A. Robb, J. R. Cheeseman, G. Scalmani, V. Barone, G. A. Petersson, H. Nakatsuji, X. Li, M. Caricato, A. V. Marenich, J. Bloino, B. G. Janesko, R. Gomperts, B. Mennucci, H. P. Hratchian, J. V. Ortiz, A. F. Izmaylov, J. L. Sonnenberg, D. Williams-Young, F. Ding, F. Lipparini, F. Egidi, J. Goings, B. Peng, A. Petrone, T. Henderson, D. Ranasinghe, V. G. Zakrzewski, J. Gao, N. Rega, G. Zheng, W. Liang, M. Hada, M. Ehara, K. Toyota, R. Fukuda, J. Hasegawa, M. Ishida, T. Nakajima, Y. Honda, O. Kitao, H. Nakai, T. Vreven, K. Throssell, J. A. Montgomery, Jr. J. E. Peralta, F. Ogliaro, M. J. Bearpark, J. J. Heyd, E. N. Brothers, K. N. Kudin, V. N. Staroverov, T. A. Keith, R. Kobayashi, J. Normand, K. Raghavachari, A. P. Rendell, J. C. Burant, S. S. Iyengar, J. Tomasi, M. Cossi, J. M. Millam, M. Klene, C. Adamo, R. Cammi, J. W. Ochterski, R. L. Martin, K. Morokuma, O. Farkas, J. B. Foresman, D. J. Fox, Gaussian 16, Revision B.01, Gaussian, Inc. Wallingford CT, **2016**.
[22] J. Tomasi, B. Mennucci, R. Cammi, *Chem. Rev.* **2005**, *105*, 2999–3094.

Manuscript received: May 1, 2023
Revised manuscript received: May 25, 2023
Accepted manuscript online: June 8, 2023
Version of record online: ■■, ■■

RESEARCH ARTICLES

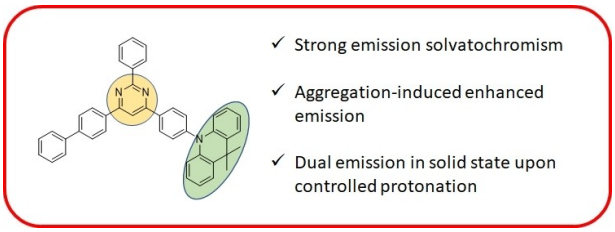

Dr. J. Massue, L. Diarra, I. Georgoulis, Dr. A. Fihey, Prof. F. Robin-le Guen, Dr. G. Ulrich, Prof. M. Fakis*, Dr. S. Achelle**

1 – 8

Aggregation-Induced Enhanced Emission of a Dimethylacridan Substituted Pyrimidine Derivative

Steady state and time-resolved spectroscopy reveal the enhanced solvatochromism, aggregation induced enhanced emission and protonation controlled dual emission of a dimethyladrydan pyrimidine chromophore.